The X-ray Outburst of H1743–322: High-Frequency QPOs with a 3:2 Frequency Ratio

Ronald A. Remillard
Center for Space Research, MIT, Cambridge, MA 02139-4307
rr@space.mit.edu
and

Jeffrey E. McClintock
Harvard-Smithsonian Center for Astrophysics, 60 Garden St. MS-3, Cambridge, MA 02138
jem@cfa.harvard.edu
and

Jerome A. Orosz
Dept. of Astronomy, San Diego State University, 5500 Campanile Drive, San Diego, CA 82182-1221
orosz@sciences.sdsu.edu
and

Alan M. Levine
Center for Space Research, MIT, Cambridge, MA 02139-4307
aml@space.mit.edu

ABSTRACT

The 2003 X-ray outburst of the candidate black-hole binary, H1743–322, was investigated in frequent pointed observations (2–250 keV) with the *Rossi* X-ray Timing Explorer. We consider one particular program of 130 observations. We organized these data into 111 time intervals and conducted a search for the presence of high-frequency quasiperiodic oscillations (HFQPOs) in the range 50–2000 Hz. Only a single observation (2003 June 13) yielded a detection above 4σ; the central frequency of 239 ± 4 Hz is consistent with the 240 Hz QPO reported for this source on 2003 May 28 (Homan et al. 2003). We next grouped the observations in several different ways and computed the average power-density spectra (PDS) in a search for further evidence of HFQPOs. This effort yielded two significant results for those observations defined by the presence of low-frequency QPOs (0.1-20 Hz) and an absence of "band-limited" power continua: (1) The 9 time intervals with the highest X-ray flux yielded an average PDS with a QPO at 166 ± 5 Hz. (4.1σ; 3–35 keV); and (2) a second group with lower X-ray flux (24 time intervals) produced an average PDS with a QPO at 242 ± 3 Hz (6.0σ; 7–35 keV). The ratio of these two frequencies is 1.46 ± 0.05. This finding is consistent with results obtained for three other black hole systems that exhibit commensurate HFQPOs in a 3:2 ratio. Furthermore, the occurrence of H1743-322's slower HFQPO at times of higher X-ray luminosity closely resembles the behavior of XTE J1550-564 and GRO J1655-40. We discuss our results in terms of a resonance model that invokes frequencies set by general relativity for orbital motions near a black-hole event horizon.

Subject headings: black hole physics — general relativity — stars: individual (H1743–322) — stars: oscillations — X-rays: stars

1. Introduction

A key question in black hole binary (BHB) research is whether high-frequency QPOs (HFQPOs), observed in the range of 40–450 Hz, represent a unique timing signature that may constrain a black hole's mass and spin via a model rooted in general relativity (GR; see McClintock & Remillard 2003). The HFQPO signals are weak, and an attack on this problem requires observations of bright X-ray transients during their rare and short-lived ($\sim$ months) outbursts.

HFQPOs have been detected in 7 confirmed or candidate BHB systems, including H1743–322 (see below). In each of three sources (GRO J1655–40, XTE J1550–564, and GRS 1915+105), transient HFQPOs have appeared at a pair of frequencies that are commensurate with a 3:2 ratio (Remillard et al. 2002a; Remillard et al. 2003). Furthermore, when the HFQPOs were compared among the three sources, it was found that the frequencies scale inversely with black hole mass. This result is consistent with expectations for oscillations produced at some characteristic radius in a strong-gravity environment described by GR theory, but only in the special case where the values of the dimensionless black hole spin parameter are similar for the three sources (McClintock & Remillard 2003).

Commensurate HFQPO frequencies can be interpreted as a signature of an oscillation driven by some type of resonance condition. Abramowicz & Kluzniak (2001) had earlier proposed that QPOs could represent enhanced emission from a particular radius where there is a resonance in the GR coordinate frequencies for orbital/epicyclic motions in strong gravity (see Merloni et al. 1999). Resonances in some form may be applicable to both BH and NS systems (Abramowicz et al. 2003). We note that GR coordinate frequencies and associated beat frequencies in the inner accretion disk were invoked in earlier work on variable-frequency QPOs in both neutron-star and some BHB systems (Stella, Vietri, & Morsink 1999).

Herein, we report on a general search for HFQPOs in the source H1743–322. The 2003 outburst of this source was first detected on March 21 in hard X-rays (15–200 keV) by INTEGRAL (IGR J17464–3213; Revnivtsev et al. 2003). Follow-up observations with *RXTE* led to the recognition that the source is a recurrent X-ray nova first observed with HEAO1 in 1977–1978 (Markwardt & Swank 2003; Gursky et al. 1978). The X-ray spectral and temporal properties exhibited during the first outburst had established H1743–322 as a black-hole candidate; its X-ray spectrum contained both a soft component (1–10 keV) and a hard X-ray tail (10–100 keV; Cooke et al. 1984), and there were no pulsations or X-ray bursts that would identify the source as a neutron-star system (Tanaka & Lewin 1995).

An X-ray light curve (1.5–12 keV) for the recent outburst is displayed in the top panel of Fig. 1, using data from the *RXTE* All-Sky Monitor (ASM; Levine et al. 1996). The bottom panel shows measurements of the spectral hardness ratio, defined as the ratio of the ASM count rate at 5–12 keV to that at 3–5 keV. These data show that the initially hard spectrum rapidly evolves to a softer one. A number of bright flares are seen before the source settles into a relatively steady and soft X-ray state. Several bright flares reach intensities near 1.5 Crab (i.e. 3.6×10^{-8} erg cm^{-2} s^{-1} at 2–10 keV) during 2003 April 18-24.

Radio detections of H1743–322 were obtained during the first few weeks of the 2003 outburst, yielding a precise celestial position and evidence for a transient radio jet (Rupen, Mioduszewski, & Dhawan 2003a; 2003b; 2003c). Soon thereafter, a faint optical counterpart was detected (R=21.9), despite $\sim$ 13 mag of dust extinction (Steeghs et al. 2003).

RXTE made 227 pointed observations of H1743–322 (=XTE J1746–326) during the 2003–2004 outburst, in the course of carrying out five different observing programs. In this paper we report on the results of a search for HFQPOs (50–2000 Hz) from this source using the 130 observations from program ID 80146. The times of these observations are indicated in the row of vertical lines in the top panel of Fig. 1. An HFQPO was reported for H1743–322 after a 25 ks observation with *RXTE* on 2003 May 28 for program ID 80135 (Homan et al. 2003). This observations yielded an HFQPO detection (4.5σ) at 240 Hz, with a possible second feature (2.5σ) at 160 Hz (Homan et al. 2003).

In the following sections we describe our analysis techniques and methods for data grouping that lead to significant detections of HFQPOs at

242 and 166 Hz. Assuming H1743–322 is a genuine BH, our discovery establishes this source as the fourth BH where a pair of HFQPOs appear to have commensurate frequencies in a 3:2 ratio. It is further be shown that additional properties of these HFQPOs bear a striking resemblance to those seen in GRO J1655–40 and XTE J1550–564 (Remillard et al. 2002a).

2. Observations and Data Analysis

We consider all of the 130 observations of H1743–322 conducted by *RXTE* under program ID 80146. This data set contains occasional sequences of short observations, and we therefore chose to collect and organize the observations into the 111 time intervals that are listed in Table 1. The number of observations combined for each time interval is given in column 4. The maximum time span for any interval is 0.48 days, and the total exposure time is 498 ks.

Our X-ray timing analyses utilize data from the *RXTE* Proportional Counter Array (PCA). The data telemetry modes chosen for this program allow us to construct PCA light curves with 125μs time resolution in 3 energy bands: 3-7, 7-14, and 14-35 keV. The PCA consists of 5 detector units (PCUs). However, the observations of H1743–322 utilized a variable number of PCUs (usually 3) because some of the PCUs are cycled off periodically to avoid problems with detector breakdown. For each observation interval, the telemetry modes for high-speed data merged all of the good events from the PCUs that were in operation.

Table 1 also provides, for each observation interval, the mean count rate (c/s/PCU) at 2-35 keV (col. 6) and at 7–35 keV (col. 7). The latter quantity is useful in evaluating the strength of nonthermal radiation in H1743–322 and was used to group observations in the search for HFQPOs. The PCA count rates are derived from background-subtracted energy spectra processed from the 'Standard 2' data mode using PCU #2, which was in use (along with PCU #0) during every observation of program 80146. All of the spectral reductions were performed via the 'ftools' routines in the HEAsoft software package distributed by NASA's HEASARC.

The procedures used to compute power density spectra (PDS) and to search for QPOs are described in Remillard et al. (2002). Briefly, for each of the 111 time intervals (Table 1), we compute Fourier transforms for each 256-s segment in the PCA light curve, and we output the average PDS for the available number of segments. We then subtract the deadtime-corrected Poisson noise and normalize the PDS to units of (rms deviation / mean)^2 Hz^{-1}. In each frequency bin, we compute the uncertainty as the larger of either the statistical error ($2/N^{0.5}$ prior to rms normalization) or the empirical standard deviation of the mean power, where N is the number of transforms (of 256 s duration) in a given observation interval. We note that this conservative approach can yield error bars that appear large, compared to bin-by-bin fluctuations, when the broad power continuum varies significantly during an observation. Finally, the power densities and uncertainties are re-binned in logarithmic intervals of frequency (ν), maintaining (for this study) a minimum $\Delta\nu/\nu = 0.04$. When we average the PDS for groups of observations, we compute the weighted mean (using σ^{-2}) and the net uncertainty for each frequency bin.

We search for HFQPOs using statistical tests to detect a Lorentzian peak rising above the local power continuum. The continuum, in terms of log P_ν, is modeled with a second order polynomial in log ν, which presumes a power-law function with allowances for broad curvature. QPOs are distinguished from broad power peaks using a coherence parameter, $Q = \nu/FWHM \gtrsim 2$. For each PDS, we use χ^2 minimization to obtain the best fit for the QPO profile and the local power continuum. Finally, in our general QPO searches, we seek results that have acceptable values of χ^2_ν while surpassing a significance threshold for the integrated QPO power (P), relative to the uncertainty (σ_P): $P/\sigma_P \gtrsim 4$. This elevated threshold compensates for the large number of PDSs and trial frequencies considered in the analysis of data sets obtained for typical bright X-ray transients.

3. Results

We searched for QPOs in the range 50–2000 Hz for each of the 111 observing intervals (Table 1). For each interval, we considered separately the average PDS for the energy ranges 3-35, 7-35, and 14-35 keV. Only one interval (2003 June 13 =

MJD 52803) yields a detection above 4σ. In this case the energy range is 7–35 keV, the central frequency is 239 ± 4 Hz, the integrated rms amplitude is $r = 2.0 \pm 0.2$ %, $Q \sim 9$, and the detection significance is 4.3 σ. The central frequency is consistent with the 240 Hz QPO detected for this source on 2003 May 28 (MJD 52787) in observations from a different *RXTE* program (Homan et al. 2003). There is one additional noteworthy finding from this initial search for HFQPOs. For the interval with highest PCA count rate (1.5 Crab on MJD 52765), an HFQPO candidate (3.8σ) appears at 162 ± 7 Hz with $Q \sim 4$ and $r = 1.1 \pm 0.2$ % (3-35 keV).

Most of the HFQPOs detections in BHB outbursts have been found in PDS averaged over a number of *RXTE* observations (Remillard et al. 1999; Cui et al. 2000; Remillard et al. 2002c) because high statistical precision is required in order to detect a faint signal spread over a bandwidth of 20 to 50 Hz. Furthermore, judicious data selection is required, since HFQPOs are usually detected only in the "steep power-law state" (McClintock & Remillard 2003), and within this state further considerations may be required to deal with amplitude variability, frequency switching, and choice of PDS energy range. We therefore investigated several strategies for grouping the observations of H1743–322 prior to further searches for HFQPO detections.

In the case of XTE J1550-564, it was shown that the phase lags (13-30 keV vs. 2-13 keV) in low-frequency QPOs (LFQPOs; 0.1-20 Hz) could be used to define three LFQPO types that are well correlated with HFQPO properties (Remillard et al. 2002c). These LFQPO types predicted, respectively, the absence of HFQPOs or the appearance of HFQPOs at either 185 or 276 Hz. We investigated this method for the case of H1743–322, but we found the results to be statistically unsatisfactory because the source is fainter than XTE J1550-564 and the LFQPO amplitudes are comparatively low.

As an alternative approach, one can capitalize on correlations found between HFQPOs and the properties of the power continuum and the energy spectrum. The LFQPO type ("C") that forecasts an absence of HFQPOs in XTE J1550-564 can also be recognized for its association with a "band-limited" power continuum in which the power density is flat at low frequencies and then drops abruptly at frequencies above the LFQPO and its harmonic. Such a PDS can be recognized via the integrated rms power derived from the PDS (0.1 to 10 Hz), and those values are given in col. 8 of Table 1. Observation intervals for H1743–322 with integrated $rms > 0.11$ all show LFQPOs and band-limited power continua, and we label these as PDS type "q-bl" in col. 9 of Table 1. Intervals with PDS that are devoid of LFQPOs are noted as PDS type "0"; these cases also exhibit the lowest values of the PCA hardness ratio (HR =col. 6 / col. 7 < 0.017, with one exception). These properties suggest that PDS type 0 designations identify the times when the source is in a thermal-dominant state (McClintock & Remillard 2003). The remaining intervals contain LFQPOs without band-limited power continua and are labeled "q" in col. 9 of Table 1.

We computed average PDS for groups "q-bl" (23 observation intervals) and "0" (44 intervals), excluding the last 9 intervals where the 2-35 keV count rate drops below 550 c/s/PCU ($\sim$ 0.2 Crab) and the PDS become statistically weak. We then divided the "q" type PDS into 2 groups distinguished by the source brightness above or below 430 c/s/PCU at 7-35 keV (col. 8 of Table 1). This latter criterion attempts to exploit the fact that the strength of the steep power-law component distinguishes the observations that yield each of the QPOs with frequencies that scale in a 3:2 ratio (hereafter referred to as the $2\nu_0$ QPO and the $3\nu_0$ QPO) in both XTE J1550-564 and GRO J1655-40 (Remillard et al. 2002a).

The PDS for the 4 groups, plotted in units of $\log(\nu \times P_\nu)$ vs. $\log \nu$, are shown in Fig. 2. The PDS fro the "q-bl" group shows a strong and very broad feature that peaks near 3 Hz. The PDS for the "0" group appears to show the same feature, although reduced in strength by a factor $\sim$ 30. HFQPO features are apparent only in the PDS for the "q" groups, and they occur at different frequencies. We note that all of the four PDS show a residual continuum above 100 Hz that is an artifact of an imperfect deadtime model for the PCA instrument.

In Fig. 3 we show the HFQPO detections for the two "q" groups at higher frequency resolution, along with the fitted models for the QPO profiles.

The 9 "q" intervals with the higher X-ray fluxes produce an average PDS (2-35 keV) with a QPO (4.1σ) at 166 ± 5 Hz, with $r = 0.60 \pm 0.08$ % and $Q = 5.7 \pm 1.6$. The "q" group comprising 26 intervals at lower X-ray flux produces an average PDS (7-35 keV) with a QPO (6.0σ) at 242 ± 3 Hz, with $r = 1.1 \pm 0.1$ % and $Q = 11 \pm 1$. Note that the transition in H1743–322 from a broader HFQPO at $2\nu_0$ in a broad bandwidth to a narrower feature at $3\nu_0$ in a harder energy band occurs with decreasing 7-35 keV count rate, which is presumably dominated by a non-thermal spectral component. This is precisely the behavior exhibited by the HFQPOs from XTE J1550-564 and GRO J1655-40 (Remillard et al. 2002a).

4. Discussion

The X-ray light curve and variability characteristics of H1743–322 during its 2003 outburst fully support the identification of this source as a black hole candidate (see §1). The behavior of H1743–322 resembles the BHBs XTE J1550-564 and GRO J1655-40 in many ways, although it was not as bright as those sources (by a factor of 3–4), comparing the brightest 4-month intervals of each outburst. This is the likely reason why we do not detect HFQPOs from H1743–322 during individual observations, other than those on MJD 52787 and possibly MJD 52765.

The effort to group the PDS in order to gain statistically significant HFQPO detections for H1743–322 was guided by results for XTE J1550-564 and GRO J1655-40 (Remillard et al. 2002a). Our best results were found simply by selecting observations with LFQPOs present, excluding cases with q-bl type power continua, and then grouping the PDS according to the 7-35 keV count rate, which represents the strength of the nonthermal X-ray flux. This effort yielded two HFQPOs with properties that closely resemble the HFQPOs of XTE J1550-564 and GRO J1655-40, i.e. the central frequencies are consistent with a 3:2 ratio, the amplitudes have $rms \sim 1\%$, and the lower frequency QPO (166 Hz for H1743–322) is seen at times of highest non-thermal flux. In addition, the higher frequency QPO (242 Hz) has a narrower profile (i.e. higher Q value) and the detection bandwidth has a relatively higher mean photon energy. We note that the one remaining BH system with HFQPOs in a 3:2 ratio (GRS 1915+105) was investigated using a different analysis method in which each QPO was extracted from a portion of a particular type of violently variable light curve (Remillard et al. 2002b; Remillard et al. 2003).

HFQPOs with frequencies at $2\nu_0$ and $3\nu_0$ can be considered as expressions of a single frequency system. As with the other BHBs discussed above, the frequency system in H1743–322 appears to be invariant through changes in luminosity or interruptions due to the source's evolution through a thermal-dominant or other states. The observations that correspond with the two groups that yield HFQPO detections (i.e. PDS type "q" in Table 1) span a range 204–1083 c/s/PCU at 7–35 keV and 1234–3775 c/s/PCU at 2–35 keV. The temporal order of these observations is shown with small arrows in the top panel of Fig. 1, where the upper/lower row represents the 242/166 Hz group, respectively. There are three gaps in the series of q-type observations (i.e. combined arrows) that occur when the PDS types are either 0 or q-bl (see Table 1).

In summary, black hole HFQPOs appear at stable pairs of frequencies with 3:2 ratio, and they exhibit common behavior patterns linked to the properties of the energy spectra. These results support the view that HFQPOs convey a distinct temporal signature for each accreting black hole. The detection bandwidth and high frequencies suggest that HFQPOs originate near the black hole event horizon. Furthermore, the stability of HFQPO pairs with changing luminosity suggests that the frequencies may depend only on the inherent properties of the black hole, viz. its mass and spin.

We have shown that the HFQPOs in H1743–322 appear to originate from the same mechanism as the HFQPOs with 3:2 frequency ratio in the other BHBs. An empirical relationship has been derived (only 3 sources) between the HFQPO frequency systems and black hole mass (McClintock & Remillard 2003), and we may apply this to the case of H1743–322. We assume that HFQPO frequencies depend only on the black hole mass (M_x) and spin, which is frequently evaluated in terms of the dimensionless spin parameter: $a_* = cJ/GM_x^2$, where J is the angular momentum of the black hole. If the black hole in H1743–322 has a similar value of a_* as the other

BHBs, then the HFQPOs (with $\nu_0 \sim 81$ Hz) suggests: $M_x = 931/\nu_0 \sim 11.5\ M_\odot$.

Detailed models of the HFQPO properties and behavior patterns must confront the problem that we do not understand the origin of the steep power-law spectrum. This radiation component is always fairly strong when the 3:2 oscillations appear. Furthermore, the strength of the steep power-law appears to regulate the frequency switching from $2\nu_0$ to $3\nu_0$.

As noted in §1, commensurate HFQPOs in BHBs have been interpreted with a "parametric resonance" concept that hypothesizes enhanced emissivity from accreting matter at a radius where two of the three coordinate frequencies (i.e. azimuthal, radial, and polar) have commensurate values that match (either directly or via beats) the observed QPO frequencies. For the cases with optical determinations of the black hole mass, the value of a_* can be determined via the application of this resonance model if the correct pair of coordinate frequencies can be identified. Reasonable values ($0.25 < a_* < 0.95$) are derived from the observed HFQPOs for either 2:1 or 3:1 ratios in either orbital:radial or polar:radial coordinate frequencies (Abramowicz & Kluzniak 2001; Remillard et al. 2002a). The driving mechanism that would allow accretion blobs to grow and survive at the resonance radius has not been specified, and it is known that there are severe damping forces in the inner accretion disk (Markovic & Lamb 1998). On the other hand, MHD accretion simulations under GR do show transient condensations in the inner disk (Hawley & Krolik 2001). Ray-tracing calculations under GR (Schnittman & Bertschinger 2004) show that the putative blobs could indeed produce the HFQPO patterns, and that the appearance of 3 ν_0 versus 2 ν_0 for the stronger QPO is governed by the angular width of the blob. Clearly, more work is needed to investigate this resonance model.

An alternative scenario is to extend the models for "diskoseismic" oscillations to include nonlinear effects that might drive some type of resonant oscillation. Diskoseismology treats the inner disk as a resonance cavity in the Kerr metric (Kato 2001; Wagoner 1999). Normal modes have been derived for linear perturbations, and the extension of this theory would be both very interesting and difficult. There are also models that invoke oscillations from geometries other than a thin disk, e.g. the accretion torus of Rezzolla et al. (2003). In any case, BHB HFQPOs deserve careful study as a potential opportunity to derive primary information about black holes while developing astrophysical applications for the strong-field regime of GR theory.

Partial support for R.R. was provided by the NASA contract to MIT for RXTE instruments. J.M. acknowledges partial support from NASA grant NAG5-10813. We thank Jeroen Homan for productive discussions about H1743-322.

REFERENCES

Abramowicz, M. A., & Kluzniak, W., 2001, A&A, 374, L19

Abramowicz, M. A., Bulik, T., Bursa, M., & Kluzniak, W., 2003 A&A, 404, L21

Cooke, B. A., Levine, A. M., Lang, F. L., Primini, F. A., & Lewin, W. G. H. 1984, ApJ, 285, 258

Cui, W., Shrader, C. R., Haswell, C. A., & Hynes, R. I. 2000, ApJ, 535, L123

Gursky et al. 1978, ApJ, 223, 973

Hawley, J.F. & Krolik, J.H. 2001, ApJ, 548, 348

Homan, J., Miller, J. M., Wijnands, R., Steeghs, D., Belloni, T., van der Klis, M., & Lewin, W. G. H. 2003, ATEL, #162

Kato, S. 2001, PASJ, 53, 1

Levine, A. M., et al. 1996, ApJ, 469, L33

Markovic, D. & Lamb, F.K. 1998, ApJ, 507, 316

Markwardt, C. B., & Swank, J. H. 2003, ATEL #136

McClintock, J. E. & Remillard, R. A. 2003, in "Compact Stellar X-ray Sources," eds. W.H.G. Lewin & M. van der Klis, (Cambridge: Cambridge U. Press), in press; astro-ph/0306213

Merloni, A., Vietri, M., Stella, L., & Bini, D. 1999, MNRAS, 304, 155

Orosz, J. A., McClintock, J. E., Remillard, R. A., & Corbel, S. 2004, ApJ, submitted; astro-ph/0404343

Parmar, A. N., Kuulkers, E., Oosterbrock, T., Barr, P., Much, R., Orr, A., Williams, O. R., & Winkler, C. 2003, A&A, 411, L421

Remillard, R. A., Morgan, E. H., McClintock, J. E., Bailyn, C. D., & Orosz, J. A. 1999, ApJ, 522, 397

Remillard, R. A., Muno, M. P., McClintock, J. E. & Orosz, J. A. 2002a, ApJ, 580, 1030

Remillard, R. A., Muno, M. P., McClintock, J. E. & Orosz, J. A. 2002b, in "New Views on Microquasars", Procs. of the 4th Microquasar Workshop, eds. Durouchoux, Fuchs, & Rodriguez, (Center for Physics: Kolkata), 57 (astro-ph/0208402)

Remillard, R. A., Sobczak, G. J., Muno, M., & McClintock, J. E. 2002c, ApJ, 564, 962

Remillard, R. A., Muno, M. P., McClintock, J. E. & Orosz, J. A. 2003, BAAS, 35, 648

Revnivtsev, M., Chernyakova, M., Capitanio, F., Westergaard, N. J., Shoenfelder, V., Gehrels, N., & Winkler, C. 2003, ATEL, #132

Rupen, M. P., Mioduszewski, A. J., & Dhawan, V. 2003, ATEL, #137

Rupen, M. P., Mioduszewski, A. J., & Dhawan, V. 2003, ATEL, #139

Rupen, M. P., Mioduszewski, A. J., & Dhawan, V. 2003, ATEL, #142

Rezzolla, L., Yoshida, S'i, Maccarone, T. J., & Zanotti, O. 2003, MNRAS, 344, L37

Schnittman, J. D. & Bertschinger, E. 2004, ApJ, in press; astro-ph/0309458

Steeghs, D., Miller, J. M., Kaplan, D., & Rupen, M. 2003, ATEL #146

Stella, L., Vietri, M. & Morsink, S. M. 1999, ApJ, 524, L63

Strohmayer, T.E. 2001, ApJ, 552, L49

Tagger, M., Varniere, P., Rodriguez, J. & Pellat, R. 2004, ApJ, in press; astro-ph/0401539

Tanaka, Y. & Lewin, W.H.G. 1995, in "X–ray Binaries", eds. W.H.G. Lewin, J. van Paradijs & E.P.J. van den Heuvel, (Cambridge:Cambridge U. Press), 126

Wagoner, R. V. 1999, Physics Reports, 311, 259

Wagoner, R. V., Silbergleit, A. S., & Ortega-Rodriguez, M. 2001, ApJ, 559, L25

This 2-column preprint was prepared with the AAS LaTeX macros v5.2.

TABLE 1
RXTE OBSERVATIONS OF H1743-322: PROGRAM 80146

#	RXTE[a] Day	MJD[b] Time	Num. Obs.	Exposure (s)	PCA Rate[c] 2-35 keV	PCA Rate[d] 7-35 keV	rms[e] (0.1-10 Hz)	PDS Type
1	3390	52743.24	1	2679	1940.2	461.5	0.112	q-bl
2	3391	52744.22	1	3059	1550.1	398.4	0.137	q-bl
3	3393	52746.20	1	2910	708.8	193.0	0.151	q-bl
4	3394	52747.63	1	3206	1024.2	247.6	0.117	q-bl
5	3397a	52750.31	2	5783	2320.3	608.2	0.050	q
6	3397b	52750.81	1	15520	2061.4	495.2	0.101	q
7	3398a	52751.09	2	6899	1660.9	384.3	0.101	q
8	3398b	52751.32	2	8406	3478.3	882.2	0.085	q
9	3398c	52751.71	1	3282	1763.3	365.6	0.104	q
10	3398d	52751.99	1	3653	1694.8	326.9	0.089	q
11	3399	52752.97	1	10764	2281.3	575.7	0.077	q
12	3400	52753.17	1	2978	2255.7	596.4	0.048	0
13	3401	52754.58	2	3542	1743.5	383.4	0.117	q-bl
14	3402	52755.96	1	7168	2637.8	414.6	0.073	q
15	3403a	52756.23	1	3541	2303.8	364.1	0.069	q
16	3403b	52756.71	1	3158	1234.5	204.2	0.074	q
17	3404	52757.80	1	6977	1108.4	136.7	0.070	0
18	3405	52758.99	1	6999	2021.7	194.9	0.055	0
19	3407a	52760.08	1	3439	1130.0	145.7	0.063	0
20	3407b	52760.56	2	3809	1152.9	145.1	0.071	0
21	3408	52761.61	1	5214	1694.6	216.0	0.066	0
22	3409	52762.75	1	6533	1733.9	256.1	0.067	0
23	3410a	52763.10	1	3418	1985.9	300.3	0.059	q
24	3410b	52763.62	1	2769	2219.5	390.0	0.061	q
25	3411	52764.91	1	6755	2228.6	392.5	0.062	q
26	3412	52765.87	1	3398	3775.2	1083.3	0.047	q
27	3413	52766.57	1	2558	1569.8	392.9	0.143	q-bl
28	3414	52767.87	1	6784	1292.2	352.2	0.159	q-bl
29	3415	52768.55	1	2154	1307.5	336.5	0.149	q-bl
30	3416	52769.75	1	2433	1227.6	326.0	0.159	q-bl
31	3417	52770.53	2	3729	1533.1	387.0	0.140	q-bl
32	3418	52771.87	2	7672	1066.5	347.5	0.192	q-bl
33	3419	52772.74	1	6068	1000.1	368.6	0.214	q-bl
34	3420	52773.73	1	6757	994.0	365.3	0.212	q-bl
35	3421	52774.58	1	6702	1036.4	330.9	0.194	q-bl
36	3422	52775.63	1	6708	953.6	339.1	0.212	q-bl
37	3423	52776.68	1	6607	712.7	280.1	0.227	q-bl
38	3424	52777.67	1	6588	979.7	333.6	0.207	q-bl
39	3425	52778.53	1	6550	1012.4	319.8	0.192	q-bl
40	3426	52779.58	2	4873	1073.7	316.4	0.186	q-bl
41	3427	52780.60	1	3395	1079.9	317.4	0.184	q-bl
42	3428	52781.62	1	6805	1046.5	314.7	0.191	q-bl
43	3429	52782.70	1	3265	1093.2	299.9	0.173	q-bl
44	3430	52783.51	1	6529	1430.5	357.0	0.129	q-bl
45	3431	52784.57	1	6721	2082.5	409.6	0.078	q
46	3432	52785.48	1	6711	2158.8	432.0	0.083	q
47	3433	52786.35	1	6433	2517.7	597.7	0.067	q
48	3435	52788.51	2	7095	1606.6	240.0	0.056	q
49	3436	52789.26	1	3477	1908.4	327.2	0.057	q
50	3437	52790.24	2	3990	1781.1	296.6	0.055	q
51	3438	52791.63	1	5796	1717.7	272.1	0.061	q
52	3439	52792.39	2	6737	1755.4	296.6	0.056	q
53	3440	52793.61	1	3138	1785.1	286.8	0.052	q
54	3441	52794.56	1	7321	2558.6	636.5	0.030	q
55	3442	52795.38	2	3741	1587.5	236.5	0.050	q
56	3443	52796.27	1	7018	1785.1	307.2	0.060	q
57	3444	52797.58	1	7159	1806.0	325.6	0.066	q

TABLE 1—*Continued*

#	RXTE[a] Day	MJD[b] Time	Num. Obs.	Exposure (s)	PCA Rate[c] 2-35 keV	PCA Rate[d] 7-35 keV	rms[e] (0.1-10 Hz)	PDS Type
58	3445	52798.54	1	3297	2647.5	675.5	0.029	q
59	3446	52799.46	1	2998	1561.3	233.7	0.048	q
60	3447	52800.73	2	11651	1528.1	215.4	0.035	q
61	3448	52801.91	1	4856	1619.8	260.7	0.055	q
62	3449	52802.96	1	4563	1614.5	272.1	0.057	q
63	3450	52803.57	1	6352	1539.1	259.6	0.058	q
64	3451	52804.62	1	6803	1607.7	298.8	0.069	q
65	3452	52805.47	1	5030	1577.6	278.3	0.063	q
66	3453	52806.63	1	3321	1361.0	187.3	0.032	0
67	3454	52807.62	1	2431	1366.3	170.1	0.033	0
68	3455	52808.64	1	5880	1311.8	162.4	0.032	0
69	3456	52809.62	1	5203	1261.5	145.1	0.033	0
70	3457	52810.54	1	5768	1137.5	101.8	0.033	0
71	3458	52811.46	2	4235	1160.8	129.1	0.035	0
72	3459	52812.67	1	4844	1132.5	120.9	0.038	0
73	3461	52814.47	1	3930	1112.8	102.3	0.027	0
74	3462	52815.84	1	3303	1003.0	77.0	0.030	0
75	3463	52816.58	1	4889	978.9	75.7	0.030	0
76	3464	52817.51	1	5704	1007.9	80.0	0.029	0
77	3465	52818.55	1	4621	994.1	74.4	0.028	0
78	3466	52819.34	2	2731	970.2	73.2	0.029	0
79	3467	52820.43	1	2418	943.9	63.6	0.029	0
80	3468	52821.42	1	2331	927.6	58.1	0.028	0
81	3469	52822.53	1	4410	922.1	57.1	0.025	0
82	3470	52823.48	1	4759	873.8	53.2	0.024	0
83	3471	52824.45	1	3329	881.8	52.1	0.027	0
84	3472	52825.37	1	2640	870.8	51.0	0.030	0
85	3473	52826.42	1	3370	893.7	54.8	0.025	0
86	3474	52827.41	1	3274	864.8	52.6	0.028	0
87	3475	52828.37	1	6712	869.0	51.7	0.026	0
88	3476	52829.28	2	5002	839.2	49.3	0.025	0
89	3477	52830.19	2	949	863.9	52.8	0.027	0
90	3478	52831.48	1	3371	860.5	51.2	0.025	0
91	3481	52834.21	2	4408	838.0	49.3	0.023	0
92	3484	52837.20	1	3492	834.4	47.4	0.024	0
93	3487	52840.56	1	2137	837.5	49.9	0.027	0
94	3490	52843.51	1	3179	816.3	52.9	0.026	0
95	3493	52846.17	2	4941	792.2	45.0	0.024	0
96	3499	52852.99	1	1770	749.2	41.0	0.027	0
97	3502	52855.54	1	3696	722.0	37.5	0.022	0
98	3509	52862.38	1	1766	668.4	35.1	0.029	0
99	3512	52865.41	1	1952	630.1	31.9	0.031	0
100	3516	52869.35	1	1463	600.6	31.1	0.032	0
101	3522	52875.12	1	1655	569.6	28.3	0.028	0
102	3524	52877.70	1	676	557.9	26.7	0.028	0
103	3530	52883.29	1	3043	511.4	24.8	0.029	0
104	3533	52886.57	1	1919	498.1	20.5	0.030	0
105	3535	52888.93	1	2342	493.6	23.3	0.023	0
106	3538	52891.43	1	2801	504.4	32.3	0.025	0
107	3541	52894.05	1	1062	489.2	31.4	0.028	0
108	3545	52898.72	1	953	426.2	26.3	0.032	0
109	3547	52900.88	1	926	419.9	19.5	0.033	0
110	3550	52903.99	1	769	392.3	19.6	0.033	0
111	3552	52905.96	1	537	385.0	22.8	0.036	0

[a]RXTE day is the mission MET time in units of truncated days.

[b]Midpoint of observation, $MJD = JD - 2,400,000.5$.

[c]Source count rate in PCA at 2–35 keV, using PCU#2.

[d]Source count rate in PCA at 7–35 keV, using PCU#2.

[e]RMS source fluctuations at 2-35 keV, integrated over the range 0.1–10 Hz, and expressed as a fraction of the average source count rate.

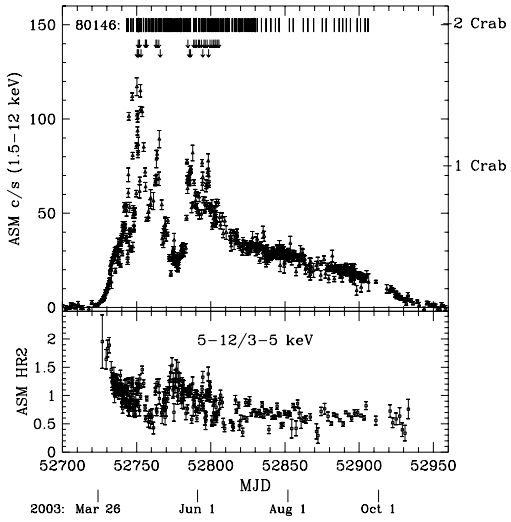

Fig. 1.— *RXTE* ASM light curve (1.5-12 keV) and hardness ratio (HR2) covering the 2003 outburst of H1743-322. For reference, the count rate for the Crab Nebula is 75.5 ASM c/s. The tick marks in the top panel indicate the times of RXTE pointed observations considered in this paper. The arrows show the times of observations contributing to QPO detections at 166 Hz (upper row) and 242 Hz (lower row), as explained in §3.

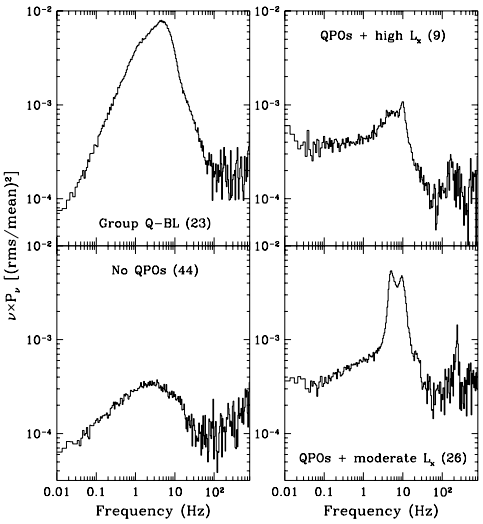

Fig. 2.— Average PDS, in units of log $(\nu \times P_\nu)$, for observations of H1743-322 grouped by the properties of the power continua and the X-ray flux. The power spectra are computed for photons in the range 2-35 keV, except for the group in the bottom-right panel, where the PDS at 7–35 keV is shown. HFQPOs are not seen when there is a band-limited power-continuum (group "Q-BL"; see text), nor when LFQPOs are absent (during times that correlate with very soft spectra). However, HFQPOs are seen (right panels) when LFQPOs are present and the band-limited power continuum is diminished. Furthermore, the HFQPOs appears to switch between two commensurate frequencies when these cases are divided into two ranges of luminosity above 7 keV.

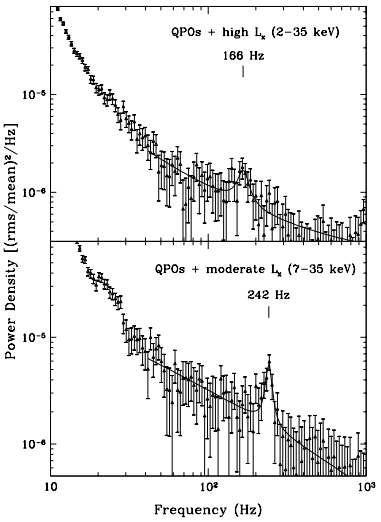

Fig. 3.— Magnified view of the high-frequency QPOs for the same two groups that have their average PDS displayed in the right panels of Fig. 2. The solid lines show the QPO profile fits, which assume a Lorentzian profile above the local power continuum. The fits are computed and displayed in units of P_ν, rather than the units of $\nu \times P_\nu$ used in Fig. 2. The central frequencies are 166 ± 5 Hz for the high L_x group at 2-35 keV, and 242 ± 3 Hz for the lower L_x group at 7-35 keV. These results are statistically consistent with an interpretation as commensurate frequencies scaled in a 3:2 ratio.